Cellular dye lasers: lasing thresholds and sensing in a planar resonator

Matjaž Humar,[1,2] Malte C. Gather[1,3] and Seok-Hyun Yun[1,4,*]

[1]*Wellman Center for Photomedicine, Harvard Medical School, Massachusetts General Hospital, 65 Landsdowne St. UP-5, Cambridge, Massachusetts 02139, USA*
[2]*Condensed Matter Department, J. Stefan Institute, Jamova 39, SI-1000 Ljubljana, Slovenia*
[3]*SUPA, School of Physics and Astronomy, University of St Andrews, St Andrews, KY16 9SS, UK*
[4]*Harvard–MIT Health Sciences and Technology, 77 Massachusetts Avenue, Cambridge, Massachusetts 02139, USA*
*syun@hms.harvard.edu

Abstract: Biological cell lasers are promising novel building blocks of future biocompatible optical systems and offer new approaches to cellular sensing and cytometry in a microfluidic setting. Here, we demonstrate a simple method for providing optical gain by using a variety of standard fluorescent dyes. The dye gain medium can be located inside or outside a cell, or in both, which gives flexibility in experimental design and makes the method applicable to all cell types. Due to the higher refractive index of the cytoplasm compared to the surrounding medium, a cell acts as a convex lens in a planar Fabry-Perot cavity. Its effect on the stability of the laser cavity is analyzed and utilized to suppress lasing outside cells. The resonance modes depend on the shape and internal structure of the cell. As proof of concept, we show how the laser output modes are affected by the osmotic pressure.

OCIS codes: (140.2050) Dye lasers; (170.1530) Cell analysis; (280.1415) Biological sensing and sensors.

References and links

1. X. Fan and S.-H. Yun, "The potential of optofluidic biolasers," Nat. Methods **11**(2), 141–147 (2014).
2. X. Fan and I. M. White, "Optofluidic microsystems for chemical and biological analysis," Nat. Photonics **5**(10), 591–597 (2011).
3. S. Nizamoglu, M. C. Gather, and S. H. Yun, "All-biomaterial laser using vitamin and biopolymers," Adv. Mater. **25**(41), 5943–5947 (2013).
4. C. Vannahme, F. Maier-Flaig, U. Lemmer, and A. Kristensen, "Single-mode biological distributed feedback laser," Lab Chip **13**(14), 2675–2678 (2013).
5. M. Chalfie, Y. Tu, G. Euskirchen, W. W. Ward, and D. C. Prasher, "Green fluorescent protein as a marker for gene expression," Science **263**(5148), 802–805 (1994).
6. R. Y. Tsien, "The green fluorescent protein," Annu. Rev. Biochem. **67**(1), 509–544 (1998).
7. D. J. Pikas, S. M. Kirkpatrick, E. Tewksbury, L. L. Brott, R. R. Naik, M. O. Stone, and W. M. Dennis, "Nonlinear saturation and lasing characteristics of green fluorescent protein," J. Phys. Chem. B **106**(18), 4831–4837 (2002).
8. M. C. Gather and S. H. Yun, "Single-cell biological lasers," Nat. Photonics **5**(7), 406–410 (2011).
9. Q. Chen, X. Zhang, Y. Sun, M. Ritt, S. Sivaramakrishnan, and X. Fan, "Highly sensitive fluorescent protein FRET detection using optofluidic lasers," Lab Chip **13**(14), 2679–2681 (2013).
10. M. C. Gather and S. H. Yun, "Bio-optimized energy transfer in densely packed fluorescent protein enables near-maximal luminescence and solid-state lasers," Nat. Commun. **5**, 5722 (2014).
11. M. C. Gather and S. H. Yun, "Lasing from Escherichia coli bacteria genetically programmed to express green fluorescent protein," Opt. Lett. **36**(16), 3299–3301 (2011).
12. A. Jonáš, M. Aas, Y. Karadag, S. Manioğlu, S. Anand, D. McGloin, H. Bayraktar, and A. Kiraz, "In vitro and in vivo biolasing of fluorescent proteins suspended in liquid microdroplet cavities," Lab Chip **14**(16), 3093–3100 (2014).
13. S. Nizamoglu, K. B. Lee, M. C. Gather, K. S. Kim, M. Jeon, S. Kim, M. Humar, and S. H. Yun, "A simple approach to biological single-cell lasers via intracellular dyes," Adv. Opt. Mater. **3**(9), 1197–1200 (2015).
14. M. Humar and S. H. Yun, "Intracellular microlasers," Nat. Photonics **9**(9), 572–576 (2015).
15. M. Humar and S.-H. A. Yun, "Microlasers inside live cells," in Proceedings of CLEO: QELS_Fundamental Science (Optical Society of America, 2015), paper JTh5A. 2.

#247953 Received 17 Aug 2015; revised 21 Sep 2015; accepted 28 Sep 2015; published 14 Oct 2015

16. M. Schubert, A. Steude, P. Liehm, N. M. Kronenberg, M. Karl, E. C. Campbell, S. J. Powis, and M. C. Gather, "Lasing within live cells containing intracellular optical micro-resonators for barcode-type cell tagging and tracking," Nano Lett. **15**(8), 5647–5652 (2015).
17. R. C. Polson and Z. V. Vardeny, "Random lasing in human tissues," Appl. Phys. Lett. **85**(7), 1289–1291 (2004).
18. P. L. Gourley, "Semiconductor microlasers: A new approach to cell-structure analysis," Nat. Med. **2**(8), 942–944 (1996).
19. P. Gourley, "Biocavity laser for high-speed cell and tumour biology," J. Phys. D Appl. Phys. **36**(14), R228–R239 (2003).
20. P. L. Gourley and R. K. Naviaux, "Optical phenotyping of human mitochondria in a biocavity laser," IEEE J. Sel. Top. Quantum Electron. **11**(4), 818–826 (2005).
21. H. Shao, D. Kumar, and K. L. Lear, "Single-cell detection using optofluidic intracavity spectroscopy," IEEE Sens. J. **6**(6), 1543–1550 (2006).
22. A. E. Siegman, *Lasers* (Mill Valley, 1986).
23. N. Lue, W. Choi, G. Popescu, Z. Yaqoob, K. Badizadegan, R. R. Dasari, and M. S. Feld, "Live cell refractometry using Hilbert phase microscopy and confocal reflectance microscopy," J. Phys. Chem. A **113**(47), 13327–13330 (2009).
24. M. H. Gassman and H. Weber, "Flashlamp-pumped high gain laser dye amplifiers," Opt. Quantum Electron. **3**(4), 177–184 (1971).
25. P. Decherchi, P. Cochard, and P. Gauthier, "Dual staining assessment of Schwann cell viability within whole peripheral nerves using calcein-AM and ethidium homodimer," J. Neurosci. Methods **71**(2), 205–213 (1997).
26. C. L. Bashford and J. C. Smith, "The use of optical probes to monitor membrane potential," Methods Enzymol. **55**, 569–586 (1979).
27. O. V. Braginskaja, V. V. Lazarev, I. N. Pershina, K. V. Petrov, L. B. Rubin, and O. V. Tikhonova, "Sodium fluorescein accumulation in cultured cells," Gen. Physiol. Biophys. **12**(5), 453–464 (1993).
28. U. T. Schwarz, M. A. Bandres, and J. C. Gutiérrez-Vega, "Observation of Ince-Gaussian modes in stable resonators," Opt. Lett. **29**(16), 1870–1872 (2004).
29. J. Homola, S. S. Yee, and G. Gauglitz, "Surface plasmon resonance sensors: review," Sens. Actuators B Chem. **54**(1–2), 3–15 (1999).
30. J. Guck, S. Schinkinger, B. Lincoln, F. Wottawah, S. Ebert, M. Romeyke, D. Lenz, H. M. Erickson, R. Ananthakrishnan, D. Mitchell, J. Käs, S. Ulvick, and C. Bilby, "Optical deformability as an inherent cell marker for testing malignant transformation and metastatic competence," Biophys. J. **88**(5), 3689–3698 (2005).

1. Introduction

The unique spectral and spatial characteristics of lasers make them useful for probing or stimulating biological cells in sensing and therapy applications. So far, the source of light for such studies has generally been an external laser that is guided to the biological sample using different forms of optics. By contrast, a recent new concept is to generate laser light within a biological material [1] by generating optical gain and resonant feedback with biomolecules, biopolymers, natural structures or synthetic biocompatible materials. Such bio-lasers have been shown to have potential for highly sensitive chemical and biological analysis [2]. Examples of biological gain media include vitamin in droplets [3] and a distributed feedback cavity [4] and green fluorescent proteins [5, 6] (GFPs) in a Fabry-Perot [7, 8] or ring resonators [9, 10]. An even more recently formed strand of research aspires to generate laser light from biomaterials *in situ* in live cells. Exploiting the fact that GFP and other fluorescent proteins can be produced by a wide variety of live organisms, live cells have been incorporated into cavities to enable lasing: For instance, GFP expressing *E. coli* bacteria were used as biological gain medium in Fabry-Perot [11] and microdroplet cavities [12], and we have shown the first biological lasers based on single human cell expressing GFP [8] or cells containing fluorescent dyes [13], using a Fabry-Perot type cavity. We have also demonstrated microcavity lasers inside cells in the form of fluorescent solid beads [14–16] or droplets, including naturally occurring lipid droplets inside adipocyte cells [14]. Random lasing has been also reported in various dye infiltrated tissues [17]. Making cells an essential part of the laser itself allows the optical characteristics of the laser output to be coupled closely with the biological properties of the cells. Since the emission of a laser is sensitive to small changes within the laser cavity [1], biological lasers can amplify changes within the cavity, making them a promising tool for biosensing applications. While having a laser cavity within a cell is beneficial for example tagging, the implanted laser could have an effect on the biological functions of the cells. Further, in the case of whispering-gallery lasers implanted in a cell that contains a functional dye only a small portion of the light generated by the dye near the surface of the cavity can be coupled into the cavity modes, while with external mirrors more

#247953 Received 17 Aug 2015; revised 21 Sep 2015; accepted 28 Sep 2015; published 14 Oct 2015

light is utilized. The sensing is also not limited to the surface of the cavity but involves the whole volume of the cell.

It has also been shown that optical properties of cells can be probed in a Fabry-Perot configuration with the cells sandwiched between a dielectric mirror and a surface-emitting semiconductor wafer providing the laser gain [18]. This method has been demonstrated for the characterization of tumor and blood cells [19] and the phenotyping of mitochondria [20]. Alternatively, the cells were also characterized using optofluidic intracavity spectroscopy by analyzing the transmitted spectrum from a broadband light source through suspension of cells in a Fabry-Perot cavity [21]. However, the gain medium was separated from the cells, and in both of the above methods the cells in the cavity merely served as passive elements altering the cavity modes. Therefore, these approaches are only sensitive to the refractive index distribution in the cells and do not use a biomaterial gain medium, such as fluorescent proteins and biocompatible dyes, which interacts with specific parts of the cells and provides biological and functional information. Combining dye functionality with a laser cavity is likely to enable applications that would not be possible when using the passive type configuration or external semiconductor gain medium.

While the use of endogenous fluorescent proteins as gain medium is fascinating, in practice it involves a somewhat long procedure: prior to the experiment, cells need to be transfected. For eukaryotes this has so far required a transient transfection approach to achieve a sufficient concentration of fluorescent protein, i.e. the plasmid encoding for GFP is not permanently introduced into the genome of the cell but instead becomes diluted as the cells proliferate. Following the transfection it typically takes about 24 hours for the intracellular concentration of fluorescent proteins to reach a peak. Furthermore, it can be challenging to achieve the fluorescent protein concentration required to thereby generate lasing and depending on the efficiency of transfection, a subsequent sorting step may be needed. Therefore, for future applications of the cell laser in sensing and imaging, a simpler approach for transforming cells into biological lasers would be beneficial.

Here, we demonstrate and characterize fluorescent organic dyes as a convenient gain medium for cell lasers. The dye molecules may be present inside or outside the cell. Such dye-based cell lasers can be made in a simple one-step procedure from virtually any type of cell. The laser output characteristics are sensitive to the number and distribution of the gain molecules, and to their emission and absorption cross-sections. In addition, our method allows us to access the huge variety of selective fluorescence-based chemical and functional probes that are already available for sensing, imaging, and cytometry. In the following, we present comprehensive design principles and characteristics of cell lasers with various dyes, cell types, and laser configurations.

2. Theory

2.1 Laser resonator stability

Low threshold lasing requires a stable resonator, where light inside the resonator is periodically refocused and should not escape from the gain region. Normally, a resonator with two plane parallel mirrors is weakly stable and can become unstable by small misalignment such as mirror tilt. However, a cell present in such a marginally stable cavity acts as a lens and thus can render the resonator configuration stable. The stability condition can be derived using the ABCD matrix method [22] or by treating the cell in contact with the bottom mirror as a concave mirror.

For a roundtrip ABCD matrix

$$M = \begin{pmatrix} A & B \\ C & D \end{pmatrix} \tag{1}$$

the stability region is given as

#247953 Received 17 Aug 2015; revised 21 Sep 2015; accepted 28 Sep 2015; published 14 Oct 2015

$$-1 < \left(\frac{A+D}{2}\right) < 1. \tag{2}$$

For the cell laser, the optical cavity is described as two flat mirrors and a thick lens in contact with the bottom mirror [21] as shown in Fig. 1. The matrix for propagation of light from the bottom mirror to the top is

$$M_1 = \begin{pmatrix} 1 & L-2R \\ 0 & 1 \end{pmatrix} \begin{pmatrix} 1 & 0 \\ \frac{n_{cell}-n_0}{Rn_0} & \frac{n_{cell}}{n_0} \end{pmatrix} \begin{pmatrix} 1 & 2R \\ 0 & 1 \end{pmatrix} \begin{pmatrix} 1 & 0 \\ \frac{n_0-n_{cell}}{Rn_{cell}} & \frac{n_0}{n_{cell}} \end{pmatrix} \tag{3}$$

and the propagation back from the top to bottom

$$M_2 = \begin{pmatrix} 1 & 0 \\ \frac{n_{cell}-n_0}{Rn_0} & \frac{n_{cell}}{n_0} \end{pmatrix} \begin{pmatrix} 1 & 2R \\ 0 & 1 \end{pmatrix} \begin{pmatrix} 1 & 0 \\ \frac{n_0-n_{cell}}{Rn_{cell}} & \frac{n_0}{n_{cell}} \end{pmatrix} \begin{pmatrix} 1 & L-2R \\ 0 & 1 \end{pmatrix} \tag{4}$$

where R and n_{cell} are the cell radius and the refractive index of the cell. The roundtrip matrix is $M = M_2M_1$. For HeLa [23] cells R = 10 μm and n_{cell} = 1.371, while the refractive index of the outside medium is n_0 = 1.334. Laser resonator is stable from its smallest length of $L_{min} = 2R$ = 20 μm limited by the cell size, up to a maximum length $L_{max} = 19.5R$ = 195 μm.

Laser resonator stability can also be calculated using standard stability condition [22] for a laser with two curved mirrors by $0 \le g_1g_2 \le 1$. For our case the cell in contact with the bottom mirror can be replaced by a spherical mirror so that $g_1 = 1 - L/f_{\text{cell}}$ and $g_2 = 1$, where L is the gap between mirrors and f_{cell} is the back focal length of the cell plus the cell diameter. The stability condition therefore reads as $0 \le 1 - L/f_{\text{cell}} \le 1$. f_{cell} is derived from focal length of a ball lens as

$$f_{\text{cell}} = R\left[\frac{\frac{n_{\text{cell}}}{n_0}}{2\left(\frac{n_{\text{cell}}}{n_0}-1\right)}\right] \tag{5}$$

The calculated focal length of the cell is f_{cell} = 195 μm. The stability region is exactly the same as calculated by the above ABCD matrix method.

For fundamental Gaussian mode, the spot size at different positions along the cavity and the spot size at the beam waist can be calculated from the g-factors [22]. The spot size at the bottom mirror w_1 is given by

$$w_1^2 = \frac{L\lambda}{\pi}\sqrt{\frac{1}{g_1(1-g_1)}} \tag{6}$$

and the spot size at the top mirror w_2 is equal to spot size at the beam waist w_0 and is given by

$$w_2^2 = w_0^2 = \frac{L\lambda}{\pi}\sqrt{\frac{g_1}{1-g_1}}. \tag{7}$$

For a typical gap between mirrors of 50 μm and a wavelength of 540 nm the spot sizes are w_1 = 4.4 μm and w_2 = 3.8 μm.

#247953 Received 17 Aug 2015; revised 21 Sep 2015; accepted 28 Sep 2015; published 14 Oct 2015

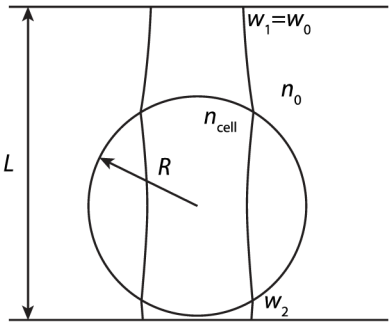

Fig. 1. Experimental configuration and parameters. A cell with radius R is placed in between mirrors with spacing L. The cell laser spot sizes at the top and bottom mirror are w_1 and w_2 respectively.

Both approaches indicate that for a typical HeLa cell the resonator length needs to be equal to or less than approximately 200 μm to achieve good stability. For most experiments in this work, the gap size was between 20 and 100 μm, so the resonator was well within the stable region and thus insensitive to small misalignments such as the two external mirrors not being completely parallel.

2.2 Lasing wavelength sensitivity to change in optical path

The wavelength of a lasing mode is dependent on the optical path length through the growth medium and the cell as

$$N\lambda = 2\left(\left(L-2R\right)n_0 + 2Rn_{cell}\right). \tag{8}$$

N is an integer number. By measuring the wavelength shift we can determine the change in the thickness and refractive index of the cell. The sensitivity is limited by how precisely the wavelength of a laser mode can be measured. The Q-factor of the cell laser (5,000) gives 0.1 nm linewidth, but due to high signal-to-noise ratio the central position of the laser line can be measured at least ten times more accurately (0.01 nm). This translates to ~20 nm sensitivity in cell thickness, for L = 25 μm and R = 20 μm. For comparison the axial resolution of a typical confocal microscope is in the order of 500 nm.

2.3 Lasing threshold

The threshold of the laser is calculated for pulsed operation in a quasi-stationary regime, since the excitation pulse (10 ns) is longer than the fluorescence lifetime (4 ns). The accumulation of triplet states is neglected in this calculation. The gain per unit length is given by [24]

$$g\left(z\right) = N\left[W\left(z\right)\tau\left(B/c + \sigma_{ss}\right) - \sigma_{ss}\right], \tag{9}$$

where N is the number concentration of dye molecules, τ is the fluorescence lifetime, c is the speed of light, σ_{ss} is the absorption cross section at the lasing wavelength,

$$B = \frac{\lambda^4 E\left(\lambda\right) n}{8\pi\tau} \quad \text{and} \quad W\left(z\right) = \frac{J\left(z\right)\sigma_0}{h\nu}, \tag{10}$$

where λ is the lasing wavelength, n is the refractive index of the medium in the cavity, $J(z)$ is the pump intensity, σ_0 is the absorption cross section at the pump wavelength, $h\nu$ is the energy of lasing photons and $E(\lambda)$ is the spontaneous lineshape function so that

$$\int_0^\infty E\left(\lambda\right) d\lambda = \phi, \tag{11}$$

#247953 Received 17 Aug 2015; revised 21 Sep 2015; accepted 28 Sep 2015; published 14 Oct 2015

ϕ being the quantum yield. In our experiment the pump intensity $J(z)$ changes with depth because of absorption by the dye because of the high numerical aperture illumination. Therefore, the gain is dependent on the z coordinate and to calculate the total gain, the intensity was numerically integrated for a roundtrip of the cavity as

$$\frac{dI}{dz} = I(z)\,g(z) \tag{12}$$

taking into account the losses at the mirrors, scattering by the cell and, if the resonator is not stabilized by a cell, also the walk-off loss. The walk-off loss increases with resonator length and misalignment angle of one mirror compared to the other. At the threshold the intensity after one roundtrip equals the initial intensity. From this condition the threshold pump power can be calculated.

3. Experimental setup

The laser cavity was made by stacking two high reflective distributed Bragg reflector (DBR) mirrors with their dielectric coating on the inside and filling the gap by a solution containing cells and a dye. For green dyes, 532 nm laser line mirrors with >99.5% reflectivity in the range 510 nm to 550 nm were used (Y2 coating, CVI) and for red dyes 633 nm laser line mirrors with >99.5% reflectivity in the range 590 nm to 700 nm were used (HN coating, CVI). The spacing between the mirrors was controlled by placing mono-disperse glass or polymer beads with sizes of 20, 30, 40, or 105 μm. The beads were deposited on the surface of one of the mirrors by sprinkling a small amount on the edges of the mirror. Alternatively for smaller beads few droplets of bead dispersion in water were deposited on the mirror and the water was let to evaporate leaving a monolayer of beads. The second mirror was placed on top leaving a thin air gap. A dispersion of cells premixed with a dye was pipetted to the edge of the two mirrors so that the dispersion filled the gap between the mirrors by capillary suction. The exact gap was calculated from the spectral separation of consecutive longitudinal lasing modes. The relative angle of the two mirrors was determined by measuring the longitudinal mode spacing at different locations of cavity. For optical pumping and light collection a 40 × 0.6-NA objective lens was used. Pumping was achieved using an optical parametric oscillator with 5 ns pulse duration, tuned to 475 nm for green dyes and to 535 nm for red dyes. The laser beam was slightly divergent at the objective entrance pupil so that the focus at the sample was behind the objective focal plane and the beam diameter at the focal plane was approximately 20 μm wide, evenly illuminating a whole cell. The collected light was sent through a dichroic mirror and split 50:50 to a CCD camera and an imaging spectrometer (300 mm focal length, 0.1 nm resolution) as shown in Fig. 2(a).

HeLa, NIH3T3, HEK293 and EL4 cell lines were used in this study. Cells were grown at 37 °C with 5% CO_2 in full growth medium (DMEM medium supplemented with 10% fetal bovine serum and 1% pen-strep). Cells were washed with PBS, then trypsinized (except for EL4) and transferred to serum free growth medium containing a fluorescent dye. The following dyes were used: 100 μM Calcein-AM (Life Technologies), 1 mM fluorescein sodium salt (Sigma-Aldrich), 3 mM Pyrromethene 556 (Exciton Inc), 1 mM Rhodamine 6G (Sigma-Aldrich) and 2 wt% Fluorescein isothiocyanate-dextran (FITC-dextran, MW 2,000,000, Sigma-Aldrich). The cells were incubated with the dye solution at standard growth conditions for 30 min and then transferred into the space between the mirrors. For FITC-dextran the cell dispersion was used immediately without incubation. Red blood cells were collected from a mouse according to protocols in compliance with institutional guidelines and approved by the Institutional Animal Care and Use Committee (IACUC) at the Harvard Medical School, and diluted 1:10 with PBS containing 1mM fluorescein sodium salt dye.

Consider an external-cavity cell laser comprised of a cell, gain medium, and a Fabry-Perot cavity based on a pair of mirrors as shown in Fig. 2(b). We discuss three configurations which differ with regards to the location of the gain medium: Type I in Fig. 2(c), with the dye only inside the cell, Type II in Fig. 2(d), with the dye only in the medium surrounding the cell and

#247953 Received 17 Aug 2015; revised 21 Sep 2015; accepted 28 Sep 2015; published 14 Oct 2015

Type III in Fig. 2(e), with the dye both inside and outside of the cell. The dye location depends on cellular uptake and therefore depends on the dye, the cell type and the state of cells – for example dyes used for viability assays enter either only dead or only viable cells [25]. Different dye configurations also have advantages and disadvantages regarding laser gain, photobleaching and staining procedure. For Type II and Type III lasers, the dye surrounding the cell contributes to the laser gain and this dye is continuously exchanged by diffusion which reduces photobleaching effects. Furthermore, if the dye is present only outside of the cell (Type II) there is no need for a staining procedure; instead the cells are simply mixed with a buffer containing the dye. Once the lasing experiment is complete, the buffer containing the dye can be easily removed and the cells can be investigated further using other analytical methods.

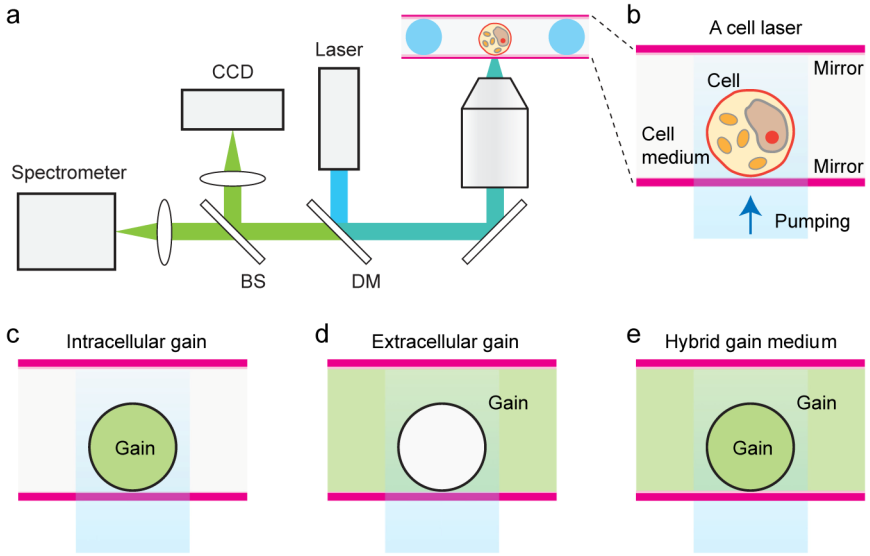

Fig. 2. Configuration of the cell laser experiments. (a) Cell lasers are pumped by an external laser through a microscope objective. The fluorescent light collected through the same objective, separated by a dichroic mirror and sent to the spectrometer and the camera. (b) Cells are placed in between two highly reflective mirrors and sink to the surface of the bottom mirror. The cell is illuminated in such way that the entire cell or a group of cells is pumped. Three gain configurations are proposed: The fluorescent dye can be situated either (c) only inside the cell (Type I), (d) only on the outside (Type II) or (e) both inside and on the outside of the cell (Type III).

4. Results

4.1 Single cell optical loss

First light absorption and scattering by the cells was measured. Small loss is important to achieve low lasing threshold. To measure the loss, a single HeLa cell floating in PBS in a glass bottom petri dish was illuminated by a low numerical aperture (NA = 0.01) laser beam at 532 nm. The beam waist size at the sample was 20 μm, matching the diameter of the cells. The detector for the transmitted light had a numerical aperture of 0.1. All the light scattered outside this numerical aperture or absorbed by the cell was regarded as loss. For comparison, the numerical aperture of a HeLa cell calculated from cell diameter and focal length is 0.05. The detection numerical aperture was chosen so that it is slightly larger than the cell numerical aperture. The measured single pass loss of as single cell was measured to be (2.6 ± 0.5)%.

#247953 Received 17 Aug 2015; revised 21 Sep 2015; accepted 28 Sep 2015; published 14 Oct 2015

4.2 Demonstration of the three types of gain configurations

Using four different dyes, we obtained lasing from HeLa cells in all three types of laser configurations as shown in Fig. 3. The excitation pump light was provided by a nanosecond Q-switched optical parametric oscillator laser system. The cells were placed between a pair of DBR mirrors with appropriate reflection and transmission spectra, and incubated in cell medium containing dyes. A Type I laser was realized by incubating HeLa cells with Calcein-AM (100 μM) for 30 min and subsequent washing to remove excess dye in the medium. Upon optical pumping of the cells at 475 nm, laser emission was generated in a spectral range of 525 to 535 nm in Fig. 3(a). The lasing threshold was 150 nJ ± 22 nJ, corresponding to 48 mJ/cm^2 fluence covering a pumping area of ~300 μm^2 (measured at the bottom mirror). Calcein-AM becomes fluorescent only in live cells so also lasing is observed only in live cells. For a Type II laser, HeLa cells were mixed with the cell-impermeable FITC-Dextran dye (2 wt%), and the cell dispersion was introduced between cavity mirrors and characterized immediately with no subsequent incubation or washing steps. The measured FITC-Dextran concentration in the cells after 30 min of incubation in the dye is less than 1% of the concentration outside. Under the same optical pumping conditions, lasing was achieved in a 540 to 560 nm range with a threshold of 53 nJ ± 3 nJ (17 mJ/cm^2) in Fig. 3(b). Cell culture medium containing the cell-permeable dye fluorescein (1 mM) was used for a Type III laser. The cells were incubated in the dye solution for 30 min and then used without washing. The measured fluorescein concentration in the cells after 30 min of incubation is approximately 50% of the dye concentration in the extracellular medium. This is also true with high fluorescein concentration in the medium (up to 5 mM) and can be further increased by longer incubation time. Again 475 nm pumping was used, generating laser light in the 530 to 555 nm range with a threshold of 45 nJ ± 6 nJ (14 mJ/cm^2) in Fig. 3(c). In another Type III laser based on Rhodamine 6G [26], lasing was observed in 594 - 606 nm range in Fig. 3(d) with a threshold of 260 nJ ± 16 nJ (82 mJ/cm^2) at 535 nm pumping.

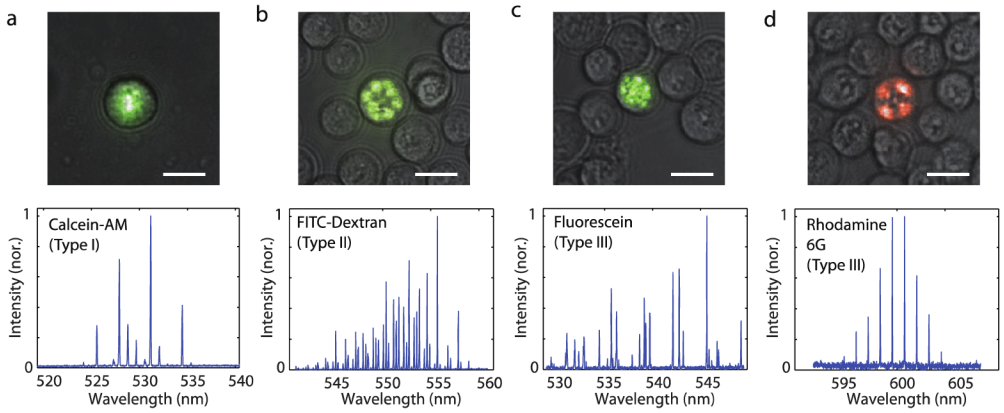

Fig. 3. Cell lasers employing different fluorescent dyes and different gain configurations. HeLa cells were suspended in a buffer containing one of four different fluorescent dyes. Top panels show an overlay of the bright field image of cells and laser emission. Lower panels show lasing spectra. (a) Calcein-AM lasing in Type I configuration where the dye is localized within the cell. (b) The very long dextran-FITC molecules do not penetrate the cell membrane forming a Type II laser. (c) Lasing of cells filled with and immersed in the green emitting dye fluorescein (Type III configuration). (d) Using the cell penetrating Rhodamine 6G, a Type III cell laser with emission in the red part of the spectrum is obtained. Scale bars, 20 μm.

To further confirm lasing, the output intensity of a single cell in fluorescein is measured as a function of input energy as shown in Fig. 4. A threshold behavior typical of lasing is observed.

#247953 Received 17 Aug 2015; revised 21 Sep 2015; accepted 28 Sep 2015; published 14 Oct 2015

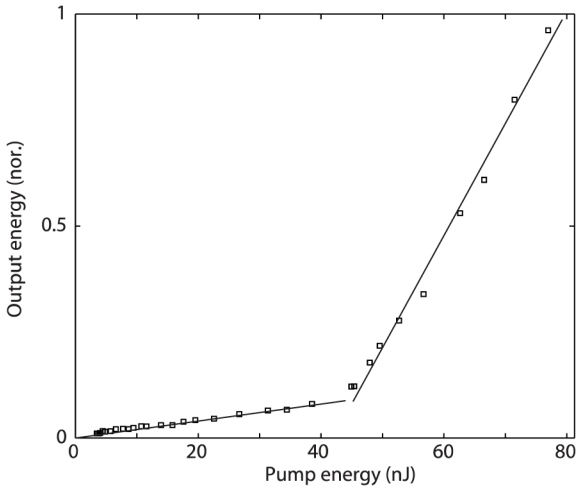

Fig. 4. Light output characteristics of a single cell shows typical threshold behavior when the pump energy is increased.

4.3 Accumulation of dye in the cells

To confirm that for FITC-Dextran we have Type II laser and for fluorescein Type III laser, the concertation of dye in cells was measured for different incubation time in media containing a dye as shown in Fig. 5. HeLa cells were detached from surface using trypsin, mixed with full growth media containing 1 mM fluorescein or 1% FITC-Dextran and incubated at growth conditions for up to 90 min. The cells were washed with PBS and their fluorescent intensity was measured using a microscope. The fluorescent intensity was compared to 1 mM fluorescein or 1% FITC-Dextran solution placed between two glass slides separated by 20 μm. For fluorescein the concentration inside the cells reaches the outside concentration in about 90 min. This is consistent with previous measurements which show accumulation of fluorescein even beyond the external concentration [27]. For FITC-Dextran the accumulation of dye is negligible even after 90 min. As a remark, the quantum yield of fluorescent dyes can be sensitive to the environment, for example pH, therefore the measurement of the fluorescence intensity may not give the exact absolute dye concentration.

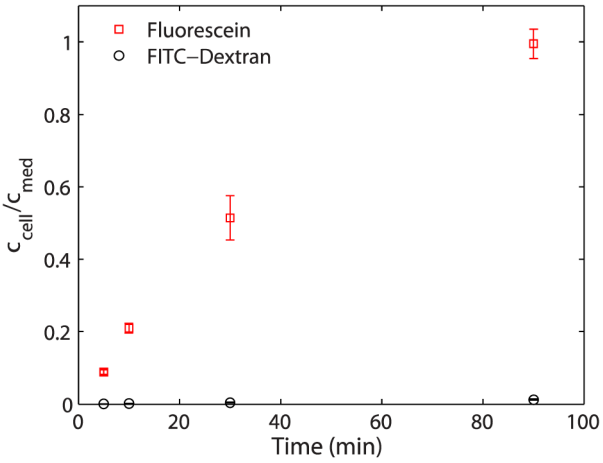

Fig. 5. Dye concentration in the cells relative to the dye concentration in the medium where the cells were incubated for different incubation times.

#247953 Received 17 Aug 2015; revised 21 Sep 2015; accepted 28 Sep 2015; published 14 Oct 2015

4.4 Lasing thresholds

Next, we investigated how the lasing thresholds changes with resonator length, dye concentration, and cavity alignment. To understand the effect of the resonator length on the lasing threshold, we measured the lasing threshold for Type-III HeLa cells in 1 mM fluorescein for different gap distances between the cavity mirrors. In the 20 – 100 μm range, the measured thresholds increased with increasing length as shown in Fig. 6(a). These results were in good agreement with calculation performed using a laser gain model [24]. The change in threshold with cavity length was caused mostly by the geometry of pumping. The size of the pump beam was smallest at the bottom mirror and increased towards the top mirror as shown in Fig. 6(d). The resonator length was adjusted by moving the upper mirror while keeping the bottom mirror fixed with respect to the pump beam. Therefore, with increasing resonator length, the size of the pump beam near the top mirror became larger, and as a result the energy density of the pump light decreased thus generating less gain. As an additional effect, the absorption loss in the cavity increased as the cavity became longer, thus also causing an overall increase in threshold.

We also measured the dependence of the lasing threshold on dye concentration at a fixed resonator length (30 μm) and found that in a range from 0.1 to 1 mM, the threshold pump energy decreased rapidly with increasing concentration as shown in Fig. 6(b). The higher dye concentration increases the gain while the losses remain nearly constant thus reducing the threshold. However, at larger concentrations from 1 to 5 mM this effect saturated, presumably primarily because the pump light is absorbed and depleted as it enters the high-concentration gain medium. This tendency is more apparent at larger resonator gaps with thicker gain medium. At concentrations above 5 mM, fluorescence quenching is expected and may cause an increase in threshold [10]. In our model, quenching was not taken into account, which explains the noticeable discrepancy between calculation and experiment at 5 mM dye concentration. We found that typically a dye concentration of 1 mM was adequate to achieve thresholds of a few tens of nJ (5-10 mJ/cm^2) and permitted prolonged laser operation with minimal photobleaching. The output power of a Type III laser with 1 mM fluorescein did not change significantly after 10,000 pump pulses at pump energy 15 times above the threshold level.

For the Type II and Type III lasers, the gain available in the space outside the cell can lead to laser emission in regions of the cavity where no cells are is present and, therefore, may generate an undesired background. This “background lasing” can be suppressed, however, by intentionally tilting the cavity mirrors to render the cavity instable in regions without cells. In our experiment with the Type III fluorescein laser, the threshold energy for background lasing (off-cell pump) increased considerably with the tilt angle, and the background lasing was completely suppressed for angles > 0.4°. By contrast, lasing threshold in Fig. 6(c) was almost independent of the tilt angle when the pumped region contained a cell due to the lens effect of cells described above. For two mirrors separated by 50 μm and at an angle of 0.5° in Fig. 6(d), a ray starting perpendicular to one of the mirrors would escape a pumped region with a width of 20 μm after only 3 round trips; on the other hand, a ray going through a cell has a stable trajectory and does not escape the gain region. At the same tilt angle of 0.5°, considering the mirror reflectivity (R > 99.5%) and the scattering loss through cells (~2.6%), the intracellular laser ray is estimated to make at least 10 round trips before its intensity falls below 50%: that is, the active finesse (Q-factor) with a cell is >100 (>5,000). This compares to <30 (<1,500) without the cell. Even without tilt in Fig. 3(c), the threshold in regions containing cells is typically about half of the threshold for background lasing, which is further evidence for the lens effect of the cell. Type II lasers are more susceptible to background lasing than Type III lasers because the lack of gain inside the cell has to be compensated. Nonetheless, we obtained background-free lasing in a Type II dextran-FITC cell laser by introducing a tilt of 0.5°.

#247953 Received 17 Aug 2015; revised 21 Sep 2015; accepted 28 Sep 2015; published 14 Oct 2015

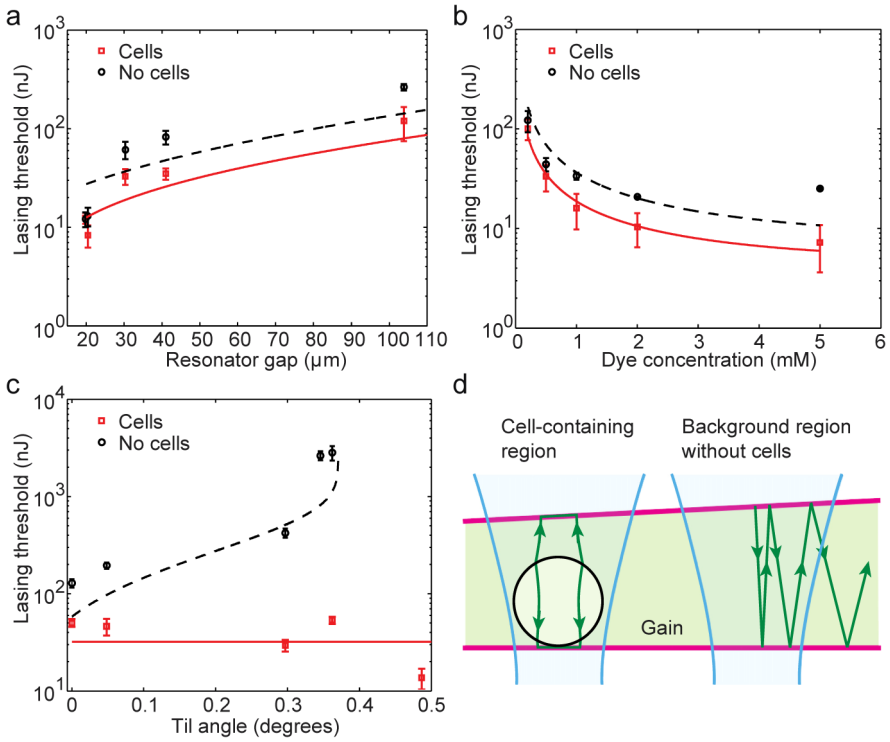

Fig. 6. Cell laser threshold with different resonator parameters. Thresholds were measured using a suspension of HeLa cells in fluorescein containing medium (Type III), either illuminating a single cell (▪) or an area of the resonator without any cells (●). Lines represent calculated thresholds for cell laser (solid red) and empty resonator (dashed black). (a) The lasing threshold gradually increases with increasing resonator gap for both cell containing and empty resonator. Concentration of fluorescein was 1 mM. (b) The threshold generally decreases with increasing fluorescein concentration, but slightly increases again at higher concentrations. Resonator gap was 30 μm. (c) For the cell laser, the threshold is nearly unaffected by the tilt angle. However, for an empty cavity the threshold increases considerably with angle and above ~0.4° lasing is not observed any longer. Resonator gap was kept constant at 50 μm and the concentration of fluorescein was 1 mM. (d) Illustration of wedged resonator design, made by tilting one mirror by a small amount (3°) with respect to the other. When a cell is present in between mirrors, the resonator remains stable, whereas with no cell present the light quickly escapes from the gain region.

4.5 Transversal lasing modes

A laser cavity can support a number of modes that can be classified as longitudinal and transverse modes. The optical path length in one round-trip equals an integer number of wavelengths, defining the fundamental frequency of each longitudinal mode. In addition, for each longitudinal mode, different transversal modes with different beam patterns exist, and in the cell laser they oscillate at different frequencies because their effective wavelengths vary by inhomogeneity in refractive index and focusing elements in the cavity. In addition, the distribution of the gain and loss in the cavity affects which of the longitudinal and transverse modes pass the threshold at given available pump energy [28]. For a uniform pump beam, the shapes of the active transversal laser modes resemble the cell shape. We used hyper-spectral imaging to separate individual oscillating modes in the spectral domain [8]. Figure 7 shows representative lasing modes of three cell types with distinctly different shapes. Laser modes from cells can be described most generally by Ince-Gaussian modes. However, spherical shaped cells in Fig. 7(a) preferentially lase in circularly symmetric Laguerre-Gaussian modes, which are solutions of the paraxial wave equation in cylindrical coordinates. Highly elongated

#247953 Received 17 Aug 2015; revised 21 Sep 2015; accepted 28 Sep 2015; published 14 Oct 2015

cells in Fig. 7(b) show Hermite-Gaussian modes, which are solutions of the paraxial wave equation in rectangular coordinates. Interestingly, because of their shape, red blood cells in Fig. 7(c) showed doughnut shaped laser modes.

To illustrate the variability of transverse modes depending on cells, we configured wide-area Type-III cell lasers based on EL4 cells and pyrromethene 556 dye. The pump beam size in Figs. 7(d) and (e) was broadened to illuminate multiple cells simultaneously. When pumped at a few tens of nJ, individual EL4 cells in Fig. 7(e) showed highly structured emission patterns corresponding to a combination of different transversal laser modes. When varying input pump energy, the output for each individual cell showed a clear threshold behavior.

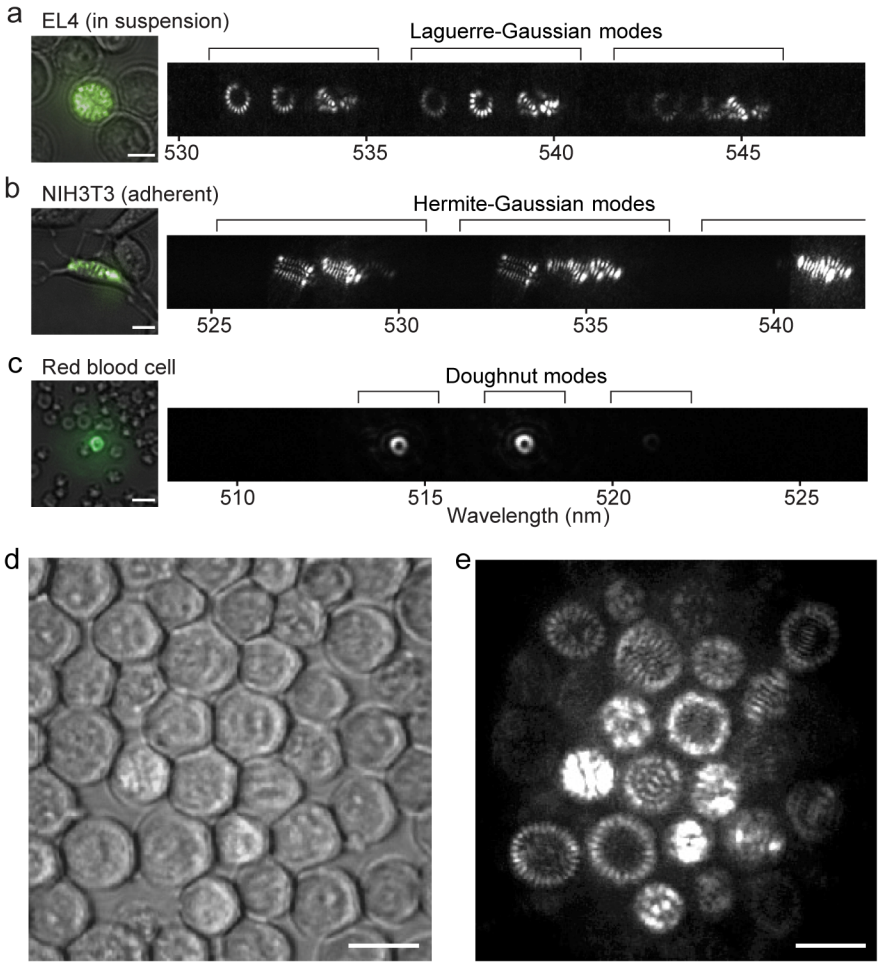

Fig. 7. Hyperspectral images of lasing modes in different cell geometries. (a-c) Overlays of bright field images and lasing images (left). Hyperspectral images of lasing modes showing both wavelength and spatial pattern of the different transverse modes (right). Lines above spectra represent groups of different transversal modes corresponding to the same longitudinal mode order. In all three cases fluorescein was used (Type III configuration) (a) Nearly spherical EL4 cell shows Laguerre-Gaussian like modes with rotational symmetry. (b) An elongated NIH3T3 cell attached to one of the mirrors lases in Hermite-Gaussian modes that resemble the elongated shape of the cell. (c) A biconcave disc shaped red blood cell also shows Laguerre-Gaussian modes. However, in this case only one of the lowest order modes with a doughnut shape is observed. Here, one mirror was tilted by 0.5° to suppress background lasing. (d) Bright-field image of a group of EL4 cells immersed in pyrromethene 556 doped buffer (Type III configuration). (e) Lasing of the same EL4 cells when illuminated by an expanded 475 nm laser beam. Scale bars, 10 μm in a, b and c, 20 μm in d and e.

#247953 Received 17 Aug 2015; revised 21 Sep 2015; accepted 28 Sep 2015; published 14 Oct 2015

4.6 Sensing

We also investigated how the modes of a single cell change when adjusting the osmolarity of the external medium. NIH3T3 cells were seeded onto a mirror fully immersed in growth medium. Cells were left for 4 h to adhere to the surface and a second mirror was sandwiched to form a laser cavity. The solution between the mirrors was exchanged by adding a small amount of medium with a pipette on one edge and collecting the old solution on the other edge. First the cells were flushed with PBS to remove any growth medium and then with 2 wt% FITC-dextran in PBS. After waiting 5 min to reach equilibrium, the lasing spectrum was captured continuously every 1 s throughout the experiment. In Fig. 8 the lasing modes of NIH3T3 cells attached to the bottom cavity mirrors were recorded over time at a pump pulse repetition rate of 10 Hz for three different conditions: (a) the cell medium was changed from PBS to pure water; (b) no stimulus; and (c) PBS was added to the cell medium inducing gentle fluid flow across the cell.

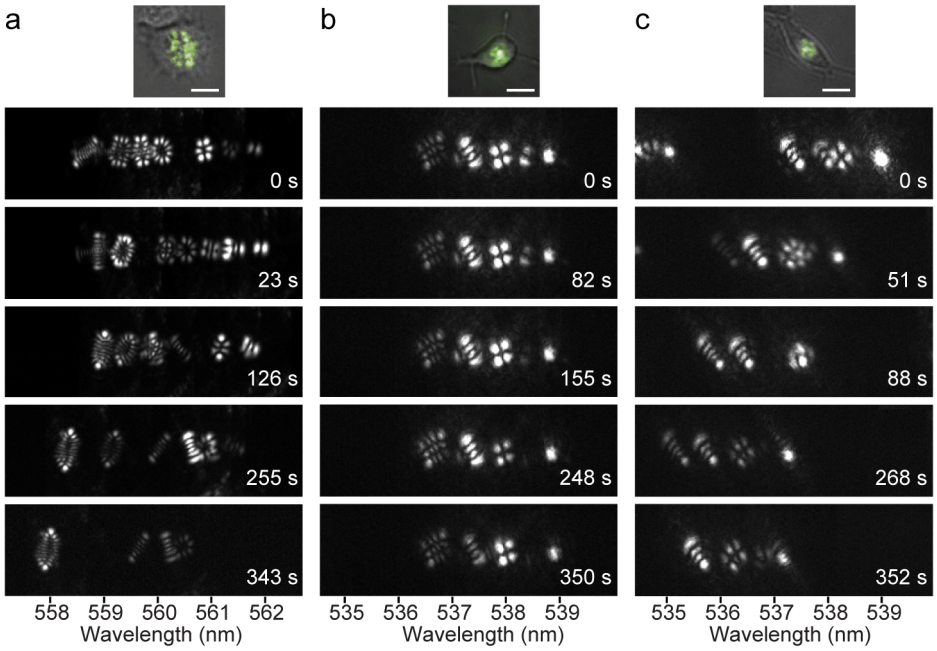

Fig. 8. Tracking changes in cell laser modes as the osmolarity of the surrounding medium is changed. Lasing modes of a single NIH3T3 cell attached to one mirror at different time points. All the modes in each case correspond to different transversal modes in a single longitudinal mode group. (a) The solution of FITC-dextran in PBS was exchanged with a solution of FITC-dextran in pure water causing the mode pattern to change dramatically, with completely different transversal modes present at the end of the experiment compared to the start. (b) Control experiment with no changes made to the solution. Modes remain stable over time, only showing a small amount of photobleaching. (c) Further control experiment in which the original solution of FITC-dextran in PBS was exchanged for an identical one. Modes change only slightly over the course of the experiment. When the flow of medium ceases, the modes return to their original structure, although at a slightly shifted wavelength due to a minute change in overall cavity thickness. Scale bars, 10 μm.

Introduction of FITC-dextran containing water into FITC-dextran containing PBS medium is expected to change osmotic pressure across the cell membrane and thereby cause an abrupt expansion of the cells. Immediately after adding the new solution, we indeed observed considerable changes in the mode structure as shown in Fig. 8(a), with some modes disappearing and new modes appearing, which we attribute to a change in cell shape. The overall spectral position of all modes also changed slightly, which is probably due to an accompanying change in the optical path length of the cavity. After 300 s, the system reached

#247953 Received 17 Aug 2015; revised 21 Sep 2015; accepted 28 Sep 2015; published 14 Oct 2015

an equilibrium where the mode pattern and position did not change any more. When no external change was induced to control cells, the modes and their spectra remained nearly constant over the course of the experiment as shown in Fig. 8(b). As a further control we exchanged the solution without changing osmolarity by injecting the same FITC-dextran in PBS mixture. In this case, the changes of the lasing modes were minimal, but an overall shift of the spectrum in Fig. 8(c) indicates that the cavity path length changes when the medium is exchanged. After equilibrium was reached again, the modes were nearly identical to the modes before addition of the medium, indicating that the previously observed effect in Fig. 8(a) was indeed caused by the variation in osmotic pressure and not only by the flow of the liquid.

5. Discussion

We have demonstrated protocols to make a cell laser based on standard cell cultures and using conventional dye staining procedures. The dye-based method shortens the incubation time required to achieve lasing to less than 1 hour, compared to 24-48 hours for the case of fluorescent proteins. A wide range of standard fluorescent cell stains can be used for the cell laser provided that they meet a minimal set of prerequisites. The cavity mirrors must be chosen appropriately for the emission of the dye and the pump wavelength. The dye can be present only inside the cells (Type I), only outside (Type II), or both inside and outside the cells (Type III) in the cavity. The lasing threshold depends on the optical properties of the dye and on the intracellular dye concentration, as well as on the cavity finesse. Our experimental and numerical results provide a general guideline for the design and operation of cell lasers and illustrate the beneficial lensing effects of a cell on the stability of a planar Fabry-Perot cavity and for reducing background lasing. Because of spherical shape of some cells they could in principle also support whispering-gallery modes (WGMs) without the need of external mirrors. However, the Q-factor of a cell as a WGM resonator is far too low to support lasing. The distance between intensity maxima observed in tangential direction shown in Figs. 3(b), 7(a) and 7(e) is several times larger than a half of the optical wavelength, which would be expected if it were to be a WGM rather than Fabry-Perot mode. Therefore, we rule out the contribution of WGMs in our experimental setting. No cell damage has been observed at the pump energy levels used throughout most of this study (less than 100 nJ). This agrees with the previous studies, which showed cell damage above approximately 1 μJ [8, 12].

For a given resonator, the transverse modes are affected by the refractive index distribution within the cell as well as by the intracellular distribution of the dye, and thus this feature can be used as a measure for cellular sensing. Compared to surface-plasmon-based sensors [29], the cell laser-based approach interrogate the changes of the cell as a whole, whereas plasmon sensors typically detect local changes very close to the sensor surface. The phenotype of a cell in the cavity plays an important role because it affects the lens effect and the distribution of the gain medium. The latter effect is generally more pronounced in Type I and Type III lasers than Types II lasers. In addition to the spatial changes, the spectral changes, such as spectral positions of the longitudinal modes, offer another sensitive metric for sensing the variations in the size and refractive index of the cell. Compared to standard fluorescence methods, placing the cells in a laser cavity amplifies the sensitivity and signal-to-noise ratio [1]. The laser output is emitted in a defined direction and can be efficiently captured by a detector whereas in the case of fluorescence, the light is emitted in all directions making detection less efficient. The ability to use standard fluorescent molecular probes may enable changing laser output in response to specific molecules or biological processes. There are numerous other probes that turn on and off or shift wavelength depending on cellular viability, cytotoxicity, pH, Ca^{2+} ion concentration, enzymes, proteins, neuron activity and so forth. Specific fluorescent probes are also designed to tag only specific part of the cell, such as cytoplasm, nucleus, mitochondria, cytoskeleton and plasma membrane. The intracellular modulation in the absorption and emission properties, quantum yield, and spatial distribution of gain molecules would manifest themselves as changes the output characteristics of the laser emission. The lasing modes could be also used to accurately measure in real time the

#247953 Received 17 Aug 2015; revised 21 Sep 2015; accepted 28 Sep 2015; published 14 Oct 2015

deformation of cells [30], either due to mechanical stress or light induced effects. The Fabry-Perot planar laser cavity considered here can be integrated with standard flow cytometry providing better overall sensitivity to the shape and the refractive index of the cells and is well suited for implementation in microfluidic chips.

Acknowledgments

This research was supported in part by the U.S. National Science Foundation (ECCS-1101947, ECCS-1505569) and National Institutes of Health (P41 EB015903). M.H. was supported in part by the Marie Curie International Outgoing Fellowship N° 627274 within the 7th European Community Framework Programme. M.C.G. was supported in part by the Starting Grant N° 640012 within the H2020 European Community Framework Programme.

#247953 Received 17 Aug 2015; revised 21 Sep 2015; accepted 28 Sep 2015; published 14 Oct 2015